



Full Length Article

On the effect of W addition on microstructural evolution and γ' precipitate coarsening in a Co–30Ni–10Al–5Mo–2Ta–2Ti alloy

Nithin Baler^{a,b,*}, Prafull Pandey^{a,*}, Dhanalakshmi Palanisamy^{a,c}, Surendra Kumar Makineni^{a,c,*}, Gandham Phanikumar^b, Kamanio Chattopadhyay^{a,*}

^a Department of Materials Engineering, Indian Institute of Science, Bangalore 560012, India

^b Department of Metallurgical and Materials Engineering, Indian Institute of Technology Madras, Chennai, India

^c Department of Microstructure Physics and Alloy Design, Max-Planck-Institute für Eisenforschung, 40237 Düsseldorf, Germany

ARTICLE INFO

Keywords:

Co-based superalloys
Partition coefficient
Atom probe tomography (APT)
Coarsening kinetics
Activation energy

ABSTRACT

The effect of replacement of molybdenum with small amount of tungsten on the stability of cobalt based superalloys of Co–Ni–Mo–Al–Ta–Ti class has been presented. A small addition of tungsten (W) in Co–30Ni–(5–x)Mo–10Al–2Ta–2Ti–2W alloys stabilizes the cuboidal morphology of precipitates and increases the γ' volume fraction. A 2 at% addition of W causes an increase of 60 °C in solvus temperature of the base superalloy to reach a value of 1130 °C with a slight increase of mass density to 8.79 g/cc. Beside partitioning into γ' , W also shifts the partitioning preference of Mo from the γ' phase in 0W alloy to that of equal partitioning in both γ and γ' phases in 2W alloy. An interfacial confinement of Mo atoms could be observed at the γ/γ' interfaces that reduces interface energy leading to enhanced microstructural stability. The experimentally determined temporal evolution of average precipitate size in the 2W alloy at the temperatures of 800, 900 and 950 °C suggests a matrix diffusion limited coarsening kinetics. The estimated coarsening rate constant at 900 °C follows a quasi-steady state model and is comparable to those observed for W and Re containing Co-based superalloys. The activation energy for γ' precipitate coarsening is estimated to be 258 ± 6 kJ/mole, which is comparable to the Mo diffusion in the γ -Co matrix suggesting Mo diffusion still controls the precipitate coarsening in the 2W alloy.

1. Introduction

The unique microstructure characteristic of L1₂ ordered γ' precipitate in γ FCC matrix in Ni-based superalloy is the main reason for the abundant use of Ni-based superalloys as high temperature structural material in turbine engines [1]. The γ - γ' microstructure provides the required property at high temperatures [2]. However, at present with the advancement of technology and desire to increase efficiency, the temperature in the turbine engines is increasing steadily. Thus, the working environment in the turbine engines is fast reaching the limit of capability of Ni-based superalloy. In order to accommodate the rise in temperature, current research concentrates on Nb and Mo as well as Co based superalloys [3,4].

The discovery of ordered γ' -Co₃(Al,W) L1₂ ordered coherent phase in Co-Al-W system [5,6], has attracted significant interest in recent time to develop high temperature structural materials as an alternative to the Ni-based superalloys. The higher solidus and liquidus tempera-

ture (50–100 °C), less segregation during solidification, acceptance of refractory elements and better sulfidation resistance than Ni-based superalloys will add up to the advantages [7–10]. The solvus temperature of Co–Al–W around 990 °C reported by Sato et al. [6] is far lower than the Ni-based superalloys while the long term thermal stability is an issue as γ' -Co₃(Al,W) phase tends to dissociates into CoAl and Co₃W equilibrium phases [11]. In order to improve the solvus temperature, thermal stability and high temperature properties, alloying additions have been carried out to the Co–Al–W alloys [7,12–16]. The studies showed that the addition of Ni, Ti and Ta to the Co–Al–W system increases the solvus temperature due to a strong partitioning preference of these elements towards γ' precipitates [17–20]. The higher solvus temperature extends the thermal stability of γ' precipitates at a higher temperature. However, the major challenges of these cobalt alloys is their high densities. The Co–Al–W and their derived alloys have densities in general greater than 9 g/cc, which are higher than Ni-based superalloys (< 9 g/cc). The requirement of higher specific strength demands

* Corresponding authors at: Department of Materials Engineering, Indian Institute of Science, Bangalore 560012, India.

E-mail addresses: nithinbaler@gmail.com (N. Baler), prafull1011@gmail.com (P. Pandey), skmakineni@iisc.ac.in (S.K. Makineni), kamanio@iisc.ac.in (K. Chattopadhyay).

Table 1

Nominal and measured compositions (in atomic%) of the studied alloys as measured by EDS in SEM.

Nominal composition (at%)	Alloy designation	Measured composition (at%)
Co-30Ni-10Al-(5-x)Mo-2Ta-2Ti-xW (x = 0.5, 1, 1.5, 2)	0.5W	50.2 ± 0.4Co - 30.6 ± 0.4Ni - 10.1 ± 0.5Al - 4.6 ± 0.2Mo - 1.9 ± 0.2Ta - 2.0 ± 0.2Ti - 0.6 ± 0.1W
	1W	50.5 ± 0.5Co - 30.3 ± 0.8Ni - 9.8 ± 0.4Al - 4.3 ± 0.3Mo - 2.0 ± 0.1Ta - 2.0 ± 0.1Ti - 1.1 ± 0.1W
	1.5W	50.6 ± 2.2Co - 30.2 ± 0.7Ni - 10.0 ± 2.2Al - 3.7 ± 0.5Mo - 1.9 ± 0.1Ta - 2.0 ± 0.2Ti - 1.6 ± 0.1W
	2W	52.4 ± 0.3Co - 30.2 ± 0.2Ni - 8.4 ± 0.9Al - 2.9 ± 0.1Mo - 1.9 ± 0.1Ta - 2.0 ± 0.1Ti - 2.2 ± 0.1W

reduction of the W concentration in Co-Al-W alloys in order to match with Ni-based superalloy. Makineni et al. have recently reported Co-Al-Mo-Nb/Ta base Co-based superalloys containing γ' -Co₃(Al,Mo,Nb/Ta) coherent cuboidal precipitates embedded uniformly in the disordered γ -Co matrix that replicates the microstructure observed in conventional Ni-based superalloys [21–23]. The mass density of this class of alloy is < 8.5 g/cc. However, these alloys suffer from lack of long-term stability due to lower solvus temperatures [24]. Therefore, in order to improve the solvus temperature, long-term stability and high temperature properties, several alloying additions such as Ni, Ti, Cr, Re have been carried out to the Co-10Al-5Mo-2Nb/Ta base alloys [18,22–26]. For example, the additions of Ni and Ti resulted in the improvement of solvus temperature to 1066 °C for a Co-10Al-30Ni-5Mo-2Ta-2Ti alloy [21]. Recently, Lass et al. have tried to develop a hybrid alloy taking advantage of the properties of both the alloys [20].

In alloys containing W, it primarily partitions and stabilizes the ordered Co₃(Al, W) γ' -L1₂ phase in fcc γ cobalt matrix. The presence of W influences the solvus temperature, alloy mass density and volume fraction of γ' precipitates in Co-Al-W system [17,19,28]. Similarly, in the W-free Co-based superalloys, besides Nb/Ta, Mo plays a major role in stabilizing the γ' ordered phase in cobalt matrix. Since W is a stronger γ' stabilizer, it is of interest to explore the effect of small amount of W replacing Mo in the Co-Al-Mo-Nb/Ta class of alloys. The present study, therefore, investigates the effect of small W addition in place of Mo in Co-30Ni-10Al-(5-x) Mo-2Ta-2Ti-xW (at.%) alloys on the alloy mass density, solvus temperature and long term microstructural stability that includes coarsening kinetics.

2. Experimental details

Alloys with nominal compositions of Co-30Ni-10Al-(5-x) Mo-2Ta-2Ti-xW at% (x = 0.5, 1, 1.5, 2), i.e., with systematically varied W content, were melted in the form of 30 g button using a vacuum arc melting unit under argon atmosphere. To achieve chemical homogeneity, each alloy was re-melted 6 to 8 times while button was flipped after each melting cycle. The as cast buttons were subsequently cast in the form of cylindrical rods with 3 mm diameter and 80 mm height using a water-cooled split copper mold that is attached with a vacuum suction unit. The bulk compositions of the alloys were measured using energy dispersive spectroscopy (EDS) detector from large number of randomly selected areas to get a better statistic. Nominal and measured composition of the alloys along with the alloy designations used in this work are presented in Table 1.

The cast rods were solutionized at 1300 °C for 24 h. This temperature is above the solvus temperature but below the temperature for incipient melting. A tubular furnace under a vacuum of 10⁻⁵ mbar was used followed by water quenching. The solutionized rods were vacuum sealed in quartz ampoules (~10⁻⁵ mbar of pressure) and aged at 900 °C for 50 h. For the study of long term microstructural stability and coarsening, the vacuum sealed solutionized samples were isothermally heat treated at 800, 900 and 950 °C for 50, 250, 500, 750 and 1000 h.

Samples for microscopic examination were prepared using Si grit papers of 1000, 1500, 2000, 2500 and 3000 grades with final polishing carried out in a Vibratory polisher (Buehler's VibroMet™ 2) using a colloidal silica solution with 250 nm particle size. The microstructural characterization of heat-treated samples was carried out using a field emission gun equipped scanning electron microscope (SEM, FEI,

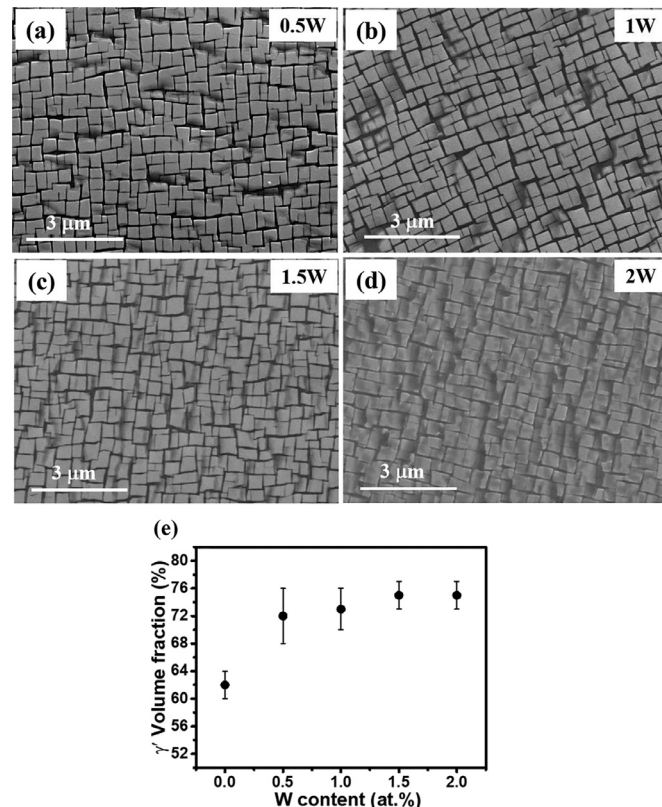


Fig. 1. Secondary electron SEM micrographs of (a) 0.5W, (b) 1W, (c) 1.5W and (d) 2W alloys subjected to aging at 900 °C for 50 h, revealing duplex γ - γ' microstructure with cuboidal shape γ' precipitates distributed uniformly within the γ matrix. (e) Change in γ' volume fraction (%) with varying W content in the alloy.

Quanta 400) operating at 20 kV in secondary electron mode. Chemical compositions of the γ and γ' phases were obtained using atom probe tomography (APT). The APT specimens were prepared from the specific site of the well-polished samples using a dual beam scanning electron microscope/focussed ion beam (FIB, Helios Nanolab 600) following an in-situ lift-out protocol, as described in Ref. [29,30]. The APT tip preparation was carried out by Ga ion milling at 30 kV in multi steps with reduction in ion current after each successive step. Finally, to remove the severely damaged surfaces of APT tip due to high energy Ga ions at 30 kV, a final cleaning was performed by Ga ion milling at 2 kV and 8 pA current. APT measurements were performed employing a reflectron equipped LEAP™ 5000XR (Cameca Instruments Inc., Madison, WI), utilizing an ultraviolet picosecond pulse laser with a pulse repetition rate of 125 kHz and a pulse energy of 50 pJ. The specimen base temperature was maintained at 50 K and the target detection rate was set to 5%, i.e., 5 detection events per 100 pulses. The data analyses of the 3-D APT reconstruction were performed using the IVAS™ 3.8.0 software package.

In order to evaluate the transformation temperature, DSC thermal analysis (DSC, STA449F3 NETSCH) was carried out for the peak-aged samples. The weighted sample of 50 mg was heated at the heating rate of 10 °C/min under Ar atmosphere till 1450 °C to allow complete

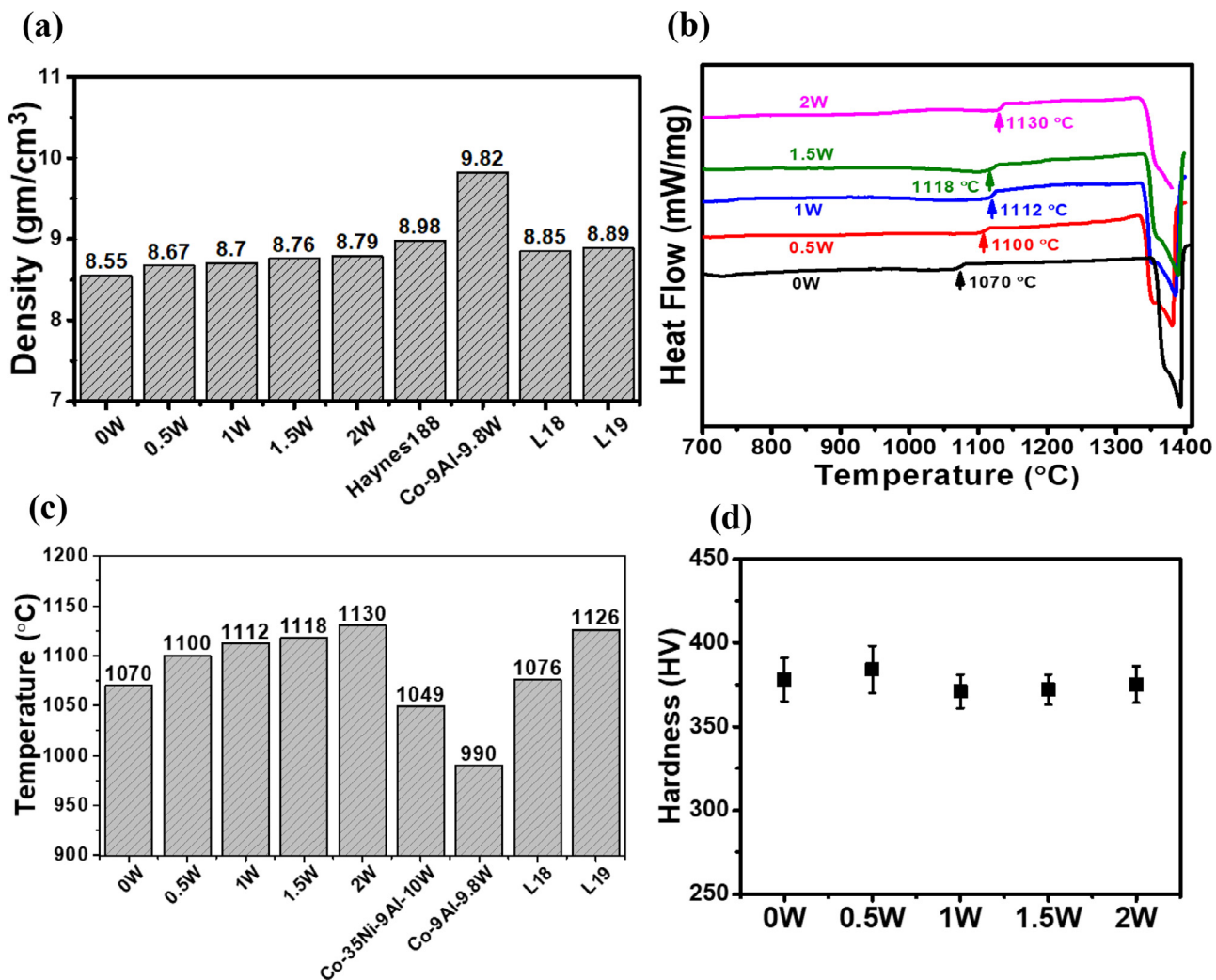


Fig. 2. (a) Bar plots comparing mass density of the 0.5W, 1W, 1.5W and 2W alloys and their comparison with Haynes 188 and other W containing Co-based superalloys. (b) Differential scanning calorimetry heating curves for the different W containing 0.5W, 1W, 1.5W and 2W alloys. (c) Bar plots comparing γ' solvus temperature of the 0.5W, 1W, 1.5W and 2W alloys and their comparison with W containing Co-based superalloys. (d) Plot showing comparison of peak hardness value during aging at 900 °C for the 0.5W, 1W, 1.5W and 2W alloys.

dissolution of γ' precipitates. Subsequently, the alloy was cooled till 50 °C at a cooling rate of 10 °C/min. The onset of first endothermic peak during heating cycle corresponds to the γ' dissolution temperature (solvus temperature). Hardness measurement on the aged samples was carried out using a Vickers microhardness tester (Future Tech, FM-800) at a load of 500 g and a dwell time of 10 s.

ASTM standard (ASTM 311-17) based on Archimedes principles was followed to determine the mass density of alloys at room temperature [31]. Prior to the measurements, the sample was cleaned using acetone and subsequently dried. γ' volume fraction measurements were carried out from [100] oriented grains following manual point count method (ASTM standard E 562-11) using the ImageJ software program. The measurement was performed on images from at least 4 different regions and average value was reported.

The precipitate size calculation was based on measuring the area (A) of each precipitate from the 2-D projected SEM images of [100] grains using the ImageJ software program. The measured area A was used to calculate the circular area equivalent radius using the following equation

$$A = \pi * r^2 \quad (1)$$

where A is the calculated γ' precipitate area and r is the circular area equivalent radius of γ' precipitate. Between 400 to 600 precipitates from

the [100] oriented grains were utilized for the average precipitate size measurement ($\langle r \rangle$). The error in average precipitate size measurement is calculated by the following equation

$$\sigma = \frac{\sigma_{std}}{\sqrt{N}} \quad (2)$$

σ is the error in average precipitate size ($\langle r \rangle$) measurement, $_{std}$ is the standard deviation of the average precipitate size and N is the number of precipitates used for the measurements.

3. Results

3.1. Microstructure

Figs. 1(a-d) shows the secondary electron SEM micrographs of the 0.5, 1W, 1.5W, and 2W alloys in their peak aging condition, i.e., aged at 900 °C for 50 h. The micrographs elucidate a uniformly distributed coherent γ' precipitates of cuboidal morphology within the γ matrix. All microstructures were obtained from the grains oriented near to the (100) type cubic direction for a consistent comparison of the morphology and size of the γ' precipitates. The edges of the cuboidal γ' precipitates are aligned along the [100] type direction, which is similar to the precipitates in the traditional Ni-based superalloys. Variation in

Table 2

Compositions (in atomic%) of the γ and γ' phases and associated partition coefficient values for 0W alloy aged at 900 °C for 50 h (taken from ref. [25]) and 2W alloy aged at 900 °C for 50 and 1000 h, as obtained by APT.

Elements	0W (900 °C for 50 h)			2W (900 °C for 50 h)			2W (900 °C for 1000 h)		
	γ	γ'	Ki	γ	γ'	Ki	γ	γ'	Ki
Co	61.90	42.32	0.68	64.04	45.71	0.71	61.03	44.98	0.74
Ni	25.70	33.98	1.32	23.58	32.08	1.36	24.93	32.49	1.30
Al	6.17	11.99	1.94	6.55	11.14	1.70	7.03	11.25	1.60
Mo	4.47	5.54	1.24	3.15	3.51	1.11	3.65	3.57	0.98
Ta	0.56	3.19	5.70	0.43	2.12	4.93	0.63	2.41	3.83
Ti	1.20	2.98	2.48	0.86	2.62	3.05	1.00	2.59	2.59
W	–	–	–	1.35	2.72	2.01	1.59	2.58	1.62

γ' volume fraction (%) with W content in the base Co-30Ni-10Al-(5-x)Mo-2Ta-2Ti-xW alloy is plotted in Fig. 1(e). An initial addition of 0.5 at% W increases the γ' volume fraction from 62 ± 2 (%) to 72 ± 4 (%) and thereafter, within the error bar, remains constant till 2 at% of W addition. This increment in γ' volume fraction with W addition was expected as W is a known γ' stabilizers in both Ni-based and W containing Co-Al-W based superalloys [17,28,32]. The γ' volume fraction for the 2W alloy is calculated to be 75 ± 2 (%). We note that Ta significantly increases the volume fraction compared to that of Nb as reported for a Co-30Ni-4Ti-2W-3Mo-1Nb-1Ta alloy [20].

3.2. Mass density, γ' solvus temperature and peak hardness value

The mass densities of different W containing alloys studied in the present investigation are plotted in Fig. 2(a). The plot also contains the densities of selected W containing Co-Al-W system as well as that of solid solution strengthened Haynes 188 [20,21]. As expected, a replacement of comparatively lighter Mo (10.2 g/cc) with heavier W (19.3 g/cc) increases the mass density from 8.55 g/cc for 0W alloy to 8.79 g/cc for 2W alloy. The mass density of present set of alloys is still lower than several other W containing Co-Al-W based systems.

Fig. 2(b) shows the DSC plots during heating cycle for the 0.5W, 1W, 1.5W and 2W alloys. The onset of first endothermic peak, i.e., γ' solvus temperature, is taken as the point of intersection between extrapolated base line and tangent at the beginning of the endothermic peak. Clearly, the γ' solvus temperature (indicated by arrow) shifts towards higher temperature with the addition of W. Fig. 2(c) shows the comparison of solvus temperature of current alloys with several other Co-based superalloys [20,21]. An addition of 2 at% W to the base 0W alloy increases the solvus temperature by 60 °C-1130 °C. The evolution of hardness values (HV) with aging time during aging at 900 °C was carried out for all alloys. The peak hardness values are plotted in Fig. 2(d). The addition of W to the 0W alloy doesn't affect the peak hardness value. Owing to superior combination of low mass density and high γ' solvus temperature, the alloy 2W is chosen for further investigations.

3.3. Compositional information across the γ/γ' interface in the 2W alloy aged at 900 °C for 50 h

Chemical information across the γ/γ' interface of the alloy 2W was obtained by carrying out atom probe tomography. Fig. 3 shows the 3D-APT reconstruction of the 2W alloy subjected to aging at 900 °C for 50 h revealing several γ' precipitates bordered by the γ matrix channel. The γ/γ' interfaces are delineated by an iso-concentration surface with a threshold value of 50 at% Co. Fig. 3 also shows the composition profiles across the γ/γ' interface for Co, Ni, Al, Ta, Ti, Mo and W elements. The profiles reveal Co-enriched γ matrix, whereas Ni, Al, Ta, Ti and W solute elements partition to the γ' precipitates. This partitioning behavior of solutes is in agreement with earlier results on Co-based superalloys [21,33-36]. The quantitative estimate of partitioning behavior of an element i across the γ/γ' interface can be obtained by the following relation

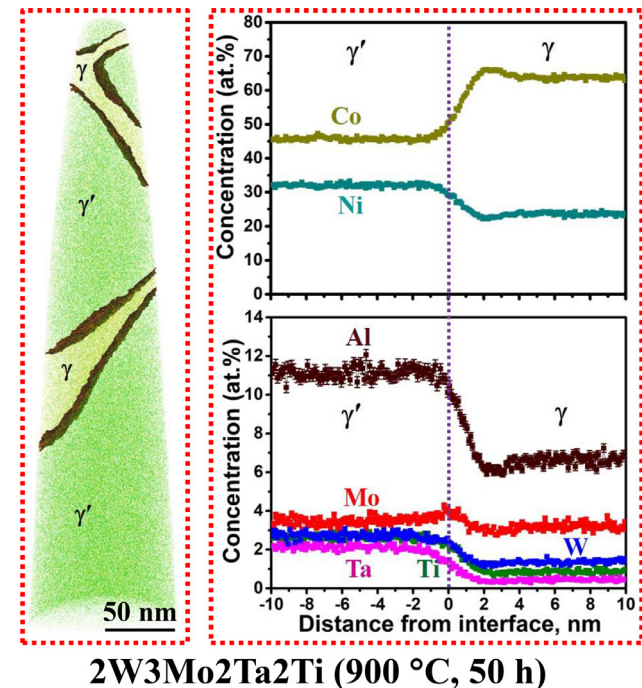


Fig. 3. 3D APT reconstruction and composition profiles across the γ/γ' interface for Co, Ni, Al, W, Mo, Ta and Ti elements in the 2W alloy subjected to aging at 900 °C for 50 h. The γ/γ' interfaces are shown as isocomposition surfaces at 50 at% Co. The inset shows enlarged view of Mo distribution across the γ/γ' interface.

$$K_i^{\gamma'/\gamma} = \frac{C_i^{\gamma'}}{C_i^{\gamma}} \quad (3)$$

where $C_i^{\gamma'}$ and C_i^{γ} are concentration of constituent element i in γ' precipitate and γ matrix and $K_i^{\gamma'/\gamma}$ is the partition coefficient of element i. Compositions of the γ and γ' phases and associated partition coefficient values for the 2W alloy and its comparison with the W free variant, 0W alloy, are presented in Table 2. Among all alloying additives, Ta and Ti partition strongly to the γ' phase with the partition coefficient values of $K_{Ta}^{\gamma'/\gamma} = 4.93$ and $K_{Ti}^{\gamma'/\gamma} = 3.05$, respectively. In contrast, Al, Ni and W shows relatively weak partitioning to the γ' phase with partition coefficient values of 1.70, 1.36 and 2.01, respectively. The γ matrix remains rich in Co with the partition coefficient ($K_{Co}^{\gamma'/\gamma}$) of 0.71. Similar partitioning behavior of these solutes was reported in the W free variant 0W alloy [25]. However, an addition of W reduces the partitioning of Mo in the γ' phase from $K_{Mo}^{\gamma'/\gamma} = 1.24$ for 0W alloy to $K_{Mo}^{\gamma'/\gamma} \sim 1.1$ for 2W alloy. Additionally, we also observed segregation of Mo atoms at the γ/γ' interface on the ordered side (see inset in Fig. 3) and a corresponding local depletion of Mo atoms in the γ matrix. Prolonged holding till 1000 h

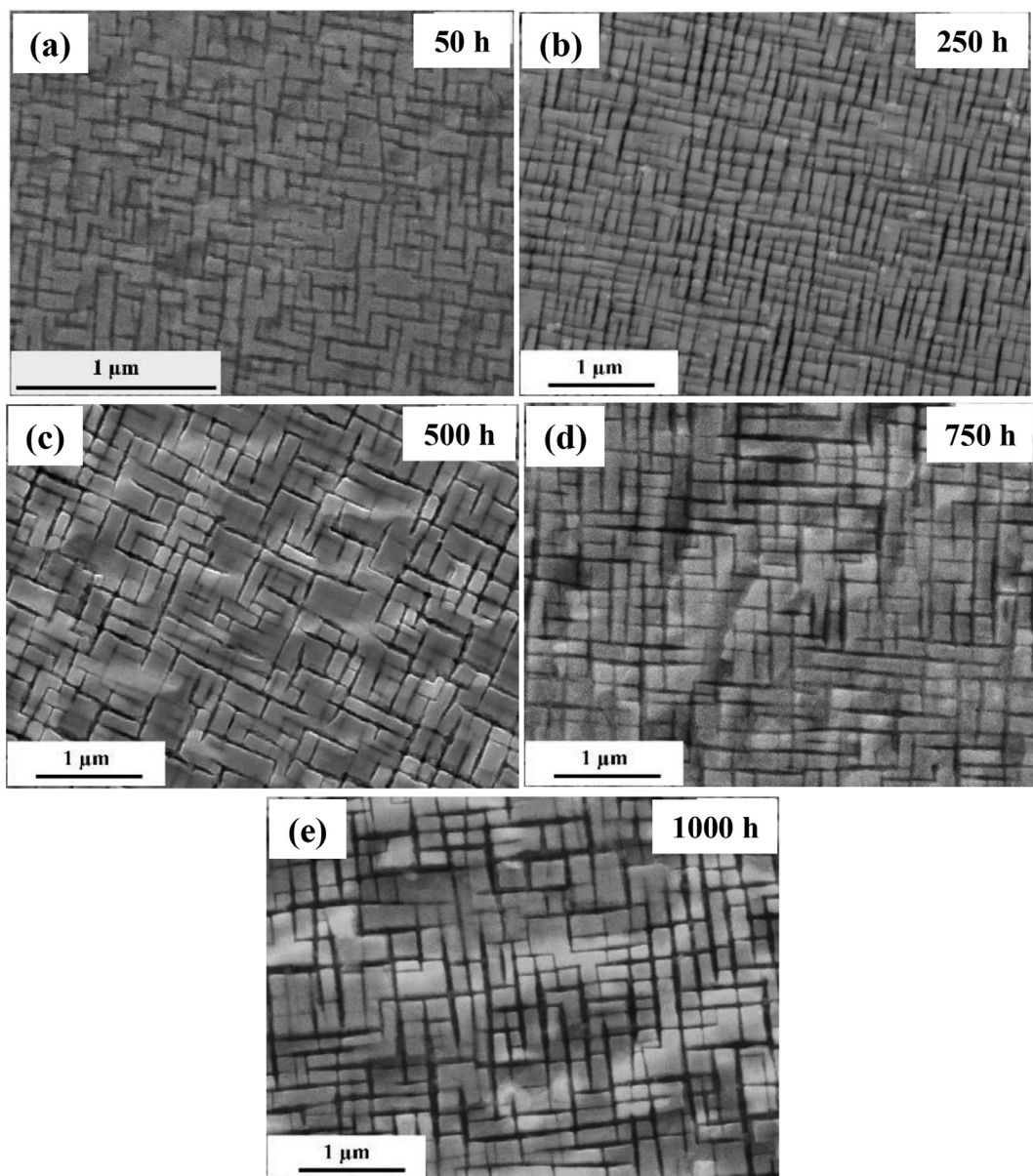


Fig. 4. Secondary electron SEM micrographs showing temporal evolution of γ - γ' microstructure of the 2W alloy during isothermal annealing at 800 °C for (a) 50, (b) 250, (c) 500, (d) 750 and (e) 1000 h.

at this temperature tends to make the $K_{Mo}^{\gamma'/\gamma}$ closer to unity. However, a slight hump in the γ' side still exist. We note that similar segregation of Mo is also observed in Nb stabilised alloy where Mo is replaced by W [20].

The total sum of Co and Ni concentration in γ' is close to 77.79 at%, which is higher than the ideal stoichiometric value of 75 at%, where Co and Ni atoms occupy the A-sites of L1₂-A₃B type unit cell. It has been reported earlier by Pandey et al. that the excess composition pertains to Co anti-sites in γ' in this class of alloys [25]. Moreover, the presence of Co anti-sites in the γ' phase is known to enhance its stability in the Co-based superalloy by shifting the fermi level towards pseudo gap [21,37,38].

3.4. Temporal evolution of γ' precipitates in the 2W alloy during isothermal exposure at 800, 900 and 950 °C

3.4.1. γ' precipitate volume fraction

The temporal evolution of γ' precipitates was studied for the 2W alloy after long term aging at different temperatures of 800, 900, and

950 °C. Figs. 4(a–e), 5(a–d), 6(a–e) show the secondary electron SEM micrographs of the samples after aging at 800, 900 and 950 °C, respectively. The micrographs were acquired from the grains oriented near to the cubic [001] direction. All the annealed samples exhibit duplex γ / γ' microstructure without formation of any other undesirable phases even along the grain boundaries. Furthermore, the γ' precipitates maintain the cuboidal morphology during aging between 50 and 1000 h at all three temperatures. However, the γ' precipitate size increases concomitantly with the inter-precipitate distance with an increase in aging time and temperature. Fig. 7(a) shows the temporal evolution of γ' precipitate volume fraction (%) during aging at 800, 900 and 950 °C. The average precipitate size obtained by averaging out the values at each aging time for the corresponding temperature is also shown as dashed line in Fig. 7(a). γ' volume fraction, within the consideration of standard deviation, remains constant thorough out the aging duration between 50 and 1000 h and slowly approaching the average volume fraction ($\bar{\phi}_{Avg}$) at all three aging temperatures. This constancy of volume suggests that the γ' precipitates have surpassed the nucleation and growth process and entered the coarsening regime. Moreover, the γ' volume fraction decreases

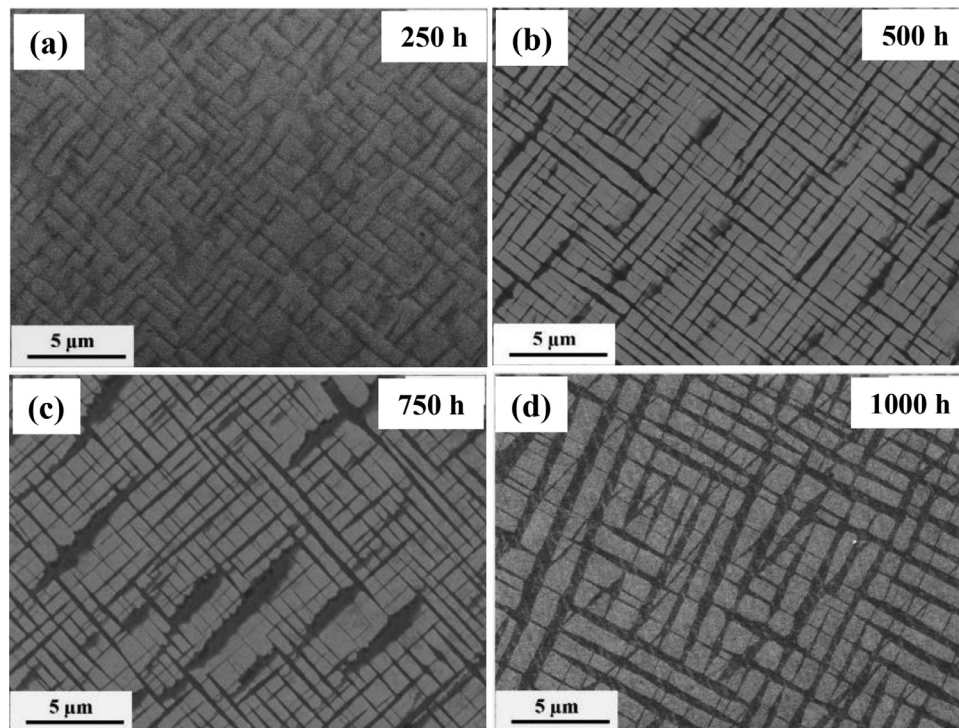


Fig. 5. Secondary electron SEM micrographs showing temporal evolution of γ - γ' microstructure of the 2W alloy during isothermal annealing at 900 °C for (a) 250, (b) 500, (c) 750 and (d) 1000 h.

from the average values of 79 (%) at 800 °C to 72 (%) at 900 °C to 67 (%) at 950 °C. This decrease in volume fraction on raising temperature was expected as the degree of solute solubility in γ -Co increases with temperature [39].

3.4.2. Precipitate morphology

From the SEM images in Figs. 4(a–e), 5(a–d) and 6(a–e), it is clear that the morphology of γ' precipitates remained cuboidal during annealing at 800, 900 and 950 °C till 1000 h. However, to evaluate the effect of coagulation or coalescence of precipitates during coarsening on γ' morphology, a parameter called ‘aspect ratio (ρ)’ has been defined. It is the ratio of the maximum circle diameter to the minimum circle diameter. Thus, for a cuboidal shaped precipitates, this ratio will be $\sqrt{2}$ while for a spheroidal precipitate it will be 1. These values were measured from 300 to 500 precipitates oriented along the [001] direction for all aging condition of the 2W alloy. The probability distribution functions of the number density of the particles with a given aspect ratio (PDF) in the microstructure are plotted with the aspect ratio (shape anisotropy) in supplementary Figs. S1(a–d), (a₁–d₁) and (a₂–d₂) for aging temperatures of 800, 900 and 950 °C. The PDF during aging at 800, 900 and 950 °C remains asymmetric and skewed towards higher values of ρ . The mean aspect ratio ($\langle \rho \rangle$) of the γ' precipitates with increasing aging time for all three aging temperature is plotted in Fig. 7(b). The $\langle \rho \rangle$ values remain close to the value of 2.0 for the aging temperatures of 800 and 900 °C. Whereas, during aging at 950 °C, the $\langle \rho \rangle$ value increases from the initial value of 1.7 after 50 h aging to close to 2.0 with further increase in aging time. However, the mode values of aspect ratio remain close to 1.5 for all aging conditions confirming the predominance of cuboidal morphology of the precipitates throughout the aging process. No rafting or preferential alignment of γ' precipitates could be observed in these alloys at all aging conditions.

3.4.3. Compositional partitioning across the γ / γ' interface after long term aging at 900 °C

3-D APT reconstruction of the 2 W alloy aged at 900 °C for 1000 h, as shown in Fig. 8, depicting γ / γ' interface, which is delineated by an iso-concentration surface with a threshold value of 50 at% Co. The com-

position profiles across the γ / γ' interface for Co, Ni, Al, Ta, Ti, Mo and W elements are shown in Fig. 8. We could observe a near complete elimination of interfacial segregation of Mo atoms that was present in the 50 h aged sample. This was expected, as the γ' precipitate growth/coarsening is limited by the matrix diffusion. Composition of the γ and γ' phases and their partition coefficient values are presented in Table 2. The change in the partition coefficient values in the 2 W during isothermal annealing at 900 °C and its comparison with 0 W alloy is shown in Fig. 9. We observe a significant change in the partition coefficient values of Ta and Mo. The partitioning of Ta reduces from $K_{Ta}^{\gamma'/\gamma} = 4.93$ after 50 h to $K_{Ta}^{\gamma'/\gamma} = 3.83$ after 1000 h. Similarly, the partitioning of Mo reduces and its partitioning preference changes from the γ' phase ($K_{Mo}^{\gamma'/\gamma} = 1.11$) in 50 h aged condition to equal distribution in both the phases ($K_{Mo}^{\gamma'/\gamma} = 0.98$) in 1000 h aged condition. Additionally, we observed that the composition profiles of all elements become flatter suggesting a possible achievement of global equilibrium of composition far away from the γ / γ' interface.

3.4.4. γ' precipitate size evolution

The temporal evolution of average precipitate size ($\langle r(t) \rangle$) for the 2 W alloy during aging at 800, 900 and 950 °C is plotted in Fig. 10(a). The plot shows a continuous increase in $\langle r(t) \rangle$ with aging time for all three temperatures. The $\langle r(t) \rangle$ values after 1000 h of aging at 800, 900 and 950 °C are calculated to be 123, 282 and 390 nm, respectively. It is to be noted that the rate of increase in $\langle r(t) \rangle$ increases with aging temperature, suggesting diffusion controlled coarsening mechanism.

3.4.5. Coarsening kinetics studies

Most of the reported γ - γ' strengthened Ni and Co-based superalloys are shown to follow matrix diffusion limited coarsening of γ' precipitates [27,34,40–44]. This was first proposed by separate works of Lifshitz and Slyozov and Wagner, commonly known as the LSW model [45,46]. The model involves growth of bigger particles at the expense of shrinking smaller particles through a process of evaporation and condensation mechanism (EC mechanism). Recently, a second mechanism for precipitate coarsening, known as TIDC model, has been proposed [47,48]. According to the TIDC model, the precipitate coarsening in the

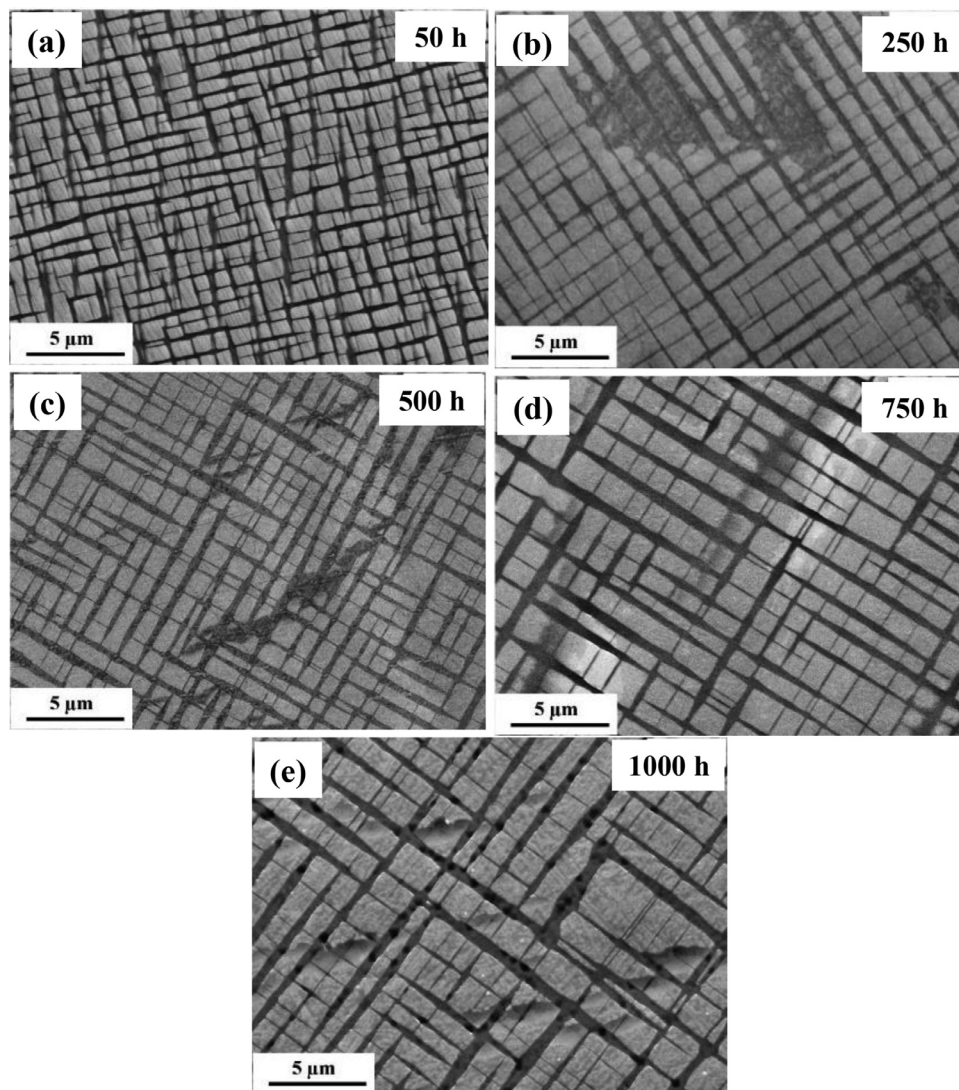


Fig. 6. Secondary electron SEM micrographs showing temporal evolution of γ - γ' microstructure of the 2W alloy during isothermal annealing at 950 °C for (a) 50, (b) 250, (c) 500, (d) 750 and (e) 1000 h.

systems involving order/disorder interface, such as γ / γ' interface in superalloys, is controlled by the solute diffusion through the partially ordered interface [48]. The operative precipitate coarsening mechanism is determined by the temporal exponent of precipitate size evolution. The exponent is expected to be close to 3 for LSW model and 2 for TIDC coarsening model. The operative coarsening mechanism in the 2W system is determined by solving the following equation

$$\langle r(t) \rangle^n - \langle r(0) \rangle^n = K_r(t - t_0) \quad (4)$$

where, $\langle r(t) \rangle$ is the average precipitate size at time t , $\langle r(0) \rangle$ is the average precipitate size at the onset of coarsening, n is the temporal exponent, K_r is the coarsening rate constant and t_0 is the time at the onset of coarsening. The unknown quantities of Eq. (4) were solved by using the linear multivariable regression analysis procedure. Fig. 10(b) shows the plots between $\log[\langle r(t) \rangle]$ vs. $\log(t)$ for all three aging temperatures. The liner regression analyses of the datasets in Fig. 10(b) give inverse of temporal exponent values ($1/n$) of 0.28 ± 0.03 , 0.23 ± 0.01 and 0.22 ± 0.02 at the aging temperatures of 800, 900 and 950 °C, respectively. These values slightly deviate from the stationary state predicted LSW model based estimated value of 0.33. Fig. 10(c) shows the plots between $\langle r(t) \rangle^3$ and t . The linear regression analysis of the datasets gives the slope values which correspond to the coarsening rate constant (K_r). The K_r values are calculated to be 0.51 , 5.8 and $15.22 \text{ nm}^3/\text{s}$ at the aging temperatures of 800, 900 and 950 °C, respectively. The temporal exponent and coarsening rate values are also presented in Table 3.

Table 3

Calculated temporal exponent ($1/n$) and coarsening rate constant (K_r) of precipitate size evolution of 2W alloy, as obtained by linear fit to the plots.

Aging temperature (°C)	Temporal exponent (1/n)	Rate constant (k_r , nm^3/s)
800	0.28 ± 0.03	0.51 ± 0.03
900	0.23 ± 0.01	5.80 ± 0.04
950	0.22 ± 0.02	15.22 ± 0.62

4. Discussion

The experimental results presented above explore the effect of replacement of Mo with small amount of W (up to 2 at%) in the Co-30Ni-10Al-5Mo-2Ta-2Ti alloy. It is shown that 2W alloy shows good γ' solvus temperature, relatively low mass density, excellent microstructural stability and coarsening resistance at elevated temperatures. Results from the present study are discussed in the context of work done by Lass et al. [20] on similar cobalt alloys containing Nb, Mo and W.

4.1. Peak aged microstructure, alloy mass density and solvus temperature

Replacing Mo with small amount of W in base alloy composition Co-30Ni-10Al-5Mo-2Ta-2Ti (at%) does not affect the cuboidal morphology of γ' precipitates. However, W addition increases the microstructural stability by increasing the γ' volume fraction from 62 ± 2 (%) for

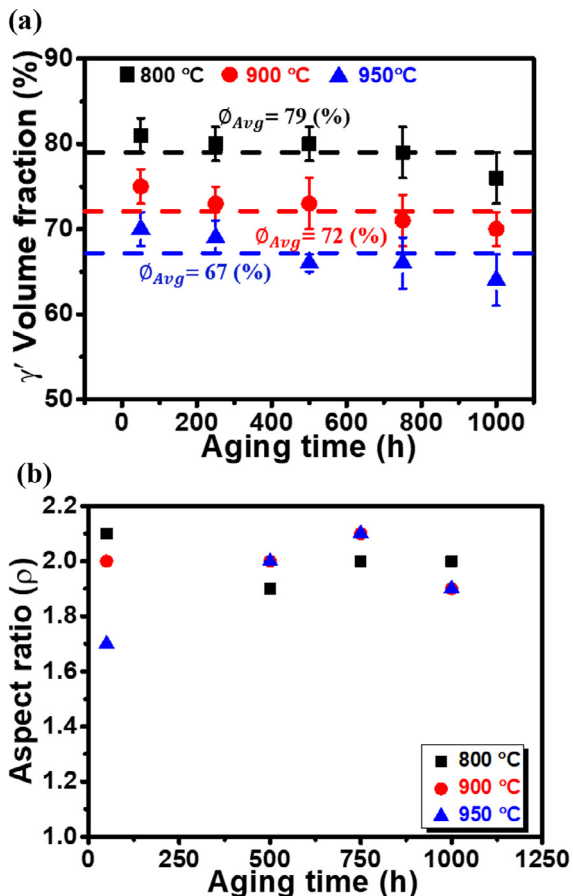


Fig. 7. Temporal evolution of (a) γ' volume fraction (%), as obtained by image analysis of [100] oriented grains and (b) aspect ratio ($r = \frac{\text{diameter of largest circle}}{\text{diameter of smallest circle}}$) for the 2W alloy subjected to annealing at 800, 900 and 950 °C. The dotted lines in (a) show average volume fraction (%) at 800, 900 and 900 °C.

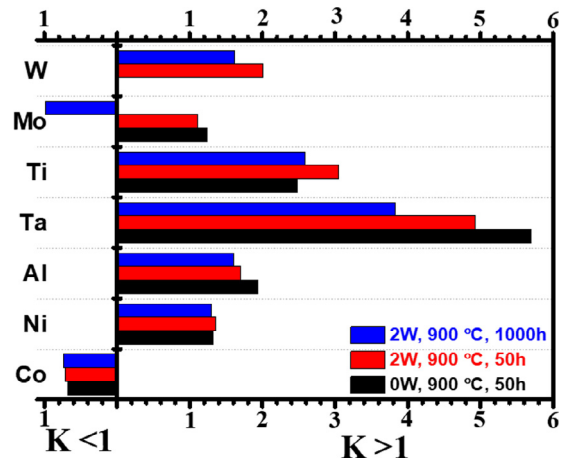
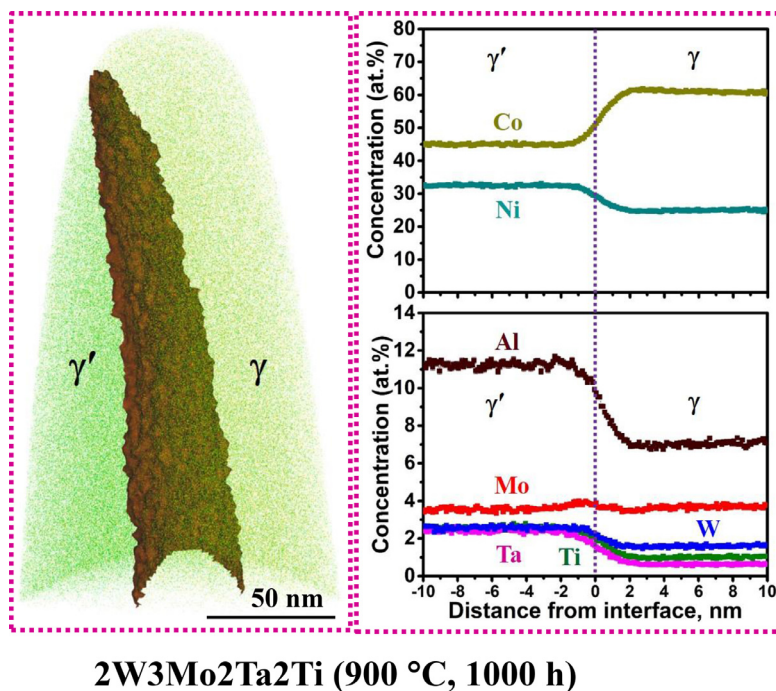


Fig. 9. Bar plots showing partition coefficient ($K_i^{\gamma'/\gamma} = \frac{C_i'}{C_i}$) of solute elements for the 0W alloy subjected to aging at 900 °C for 50 h [25] and 2W alloy subjected to annealing at 900 °C for 50 and 1000 h.

0W alloy to 75 ± 2 (%) for 2W alloy. The increase in the γ' volume fraction with W addition has already been reported in earlier work [17,28]. Lass et al. have reported that the addition of 2 at% W to the Co–Ni–Ti–Al–Mo–Nb–Ta alloy increases the γ' volume fraction from 60 (%) to 65 (%). As expected, heavier W (19.3 g/cc) replacing comparatively lighter Mo (10.2 g/cc) increases the mass density of the alloy. However, the mass densities of the present alloys are still lower than various other W containing Co-based superalloys [20,49,50]. Simultaneously with the increase in volume fraction, a 2 at% of addition of W also increases the γ' solvus temperature which is consistent with the earlier reports on the γ' solvus temperature in Co-based superalloys [17,20,28]. Pyczak et al. report an increase in γ' solvus temperature by 76 °C with increasing W content from 8 to 11 at% in the Co–9Al–xW–0.1B alloy. Similarly, Bocchini et al. have reported a rise in solvus temperature by 46 °C for every 1 at% increases in W content in the Co–10Ni–6Al–xW–6Ti alloy [51]. Both the increase in solvus temperature and volume fraction needs to



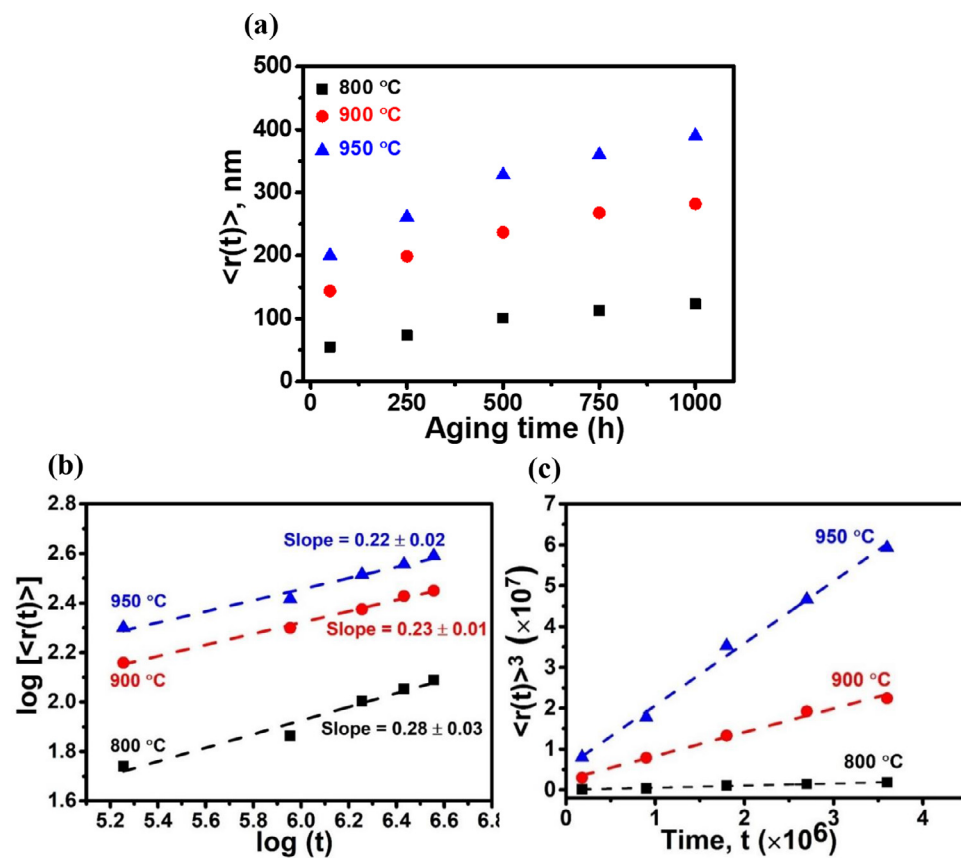


Fig. 10. (a) Temporal evolution of average precipitate size ($\langle r(t) \rangle$) for the 2W alloy subjected to annealing at 800, 900 and 950 °C. (b) Plots between $\log [\langle r(t) \rangle]$ versus $\log(t)$ for annealing temperatures of 800, 900 and 950 °C. The linear fits to the datasets give temporal exponent ($1/n$) of γ' precipitate size evolution, which are equivalent to the exponent values in classical LSW model and modified LSW model. (c) Plots between $[\langle r(t) \rangle]^3$ versus t and fit to the experimental datasets using linear regression analysis gives coarsening rate constant values at 800, 900 and 950 °C.

be viewed along with the partitioning behaviors of different elements in the γ' and γ phases.

4.2. Elemental partitioning across the γ/γ' interface for 2W alloy during aging at 900 °C

Tungsten (W), as discussed earlier, partitions and stabilizes the γ' phase. As the composition profiles, measured by APT across the γ/γ' interfaces, reveal the partitioning of most of the constituent elements in base 0W alloy and W containing 2W alloy, subjected to aging at 900 °C for 50 h, are similar to that reported in the literature for this class of alloys [21,25] and other Ni and Co-based superalloys. The strong γ' stabilizers such as Ta, Ti, Al, Ni and W partition preferentially to the γ' phase, whereas Co partitions strongly to the γ matrix [1,18,20,33,34,52–55]. In contrast, partitioning of Mo is influenced by the presence of W and attains a value closer to 1 when 2 at% W is added to the base (0W) alloy. Additionally, an interfacial segregation of Mo atoms towards the γ' side at the γ/γ' interface has been observed, as can be seen in inset of Fig. 3. The local depletion of Mo suggests matrix diffusion limited growth/coarsening of γ' precipitates. During the precipitate growth/coarsening, Mo atoms have to diffuse away from the γ/γ' interface to the γ' precipitates, but the limited diffusivity of Mo in the concentrated matrix leads to achievement of local equilibrium at the interface while global equilibrium in the matrix is not achieved yet, as can be clearly seen in Fig. 3. Further aging of alloy at 900 °C for 1000 h leads to removal of segregation and local depletion of Mo atoms with composition profiles of the γ and γ' phases become uniform. This indicates that the true equilibrium composition has been achieved. A coarsening kinetic study by Meher et al. in the Co-Al-W system reports the local depletion of W atoms in the γ matrix near the γ/γ' interface and that was wiped out with further aging [34]. Furthermore, the partition coefficient of solute elements other than Ta does not

change significantly with increase in aging time from 50 h to 1000 h. The compositions of the γ and γ' phases with associated partition coefficient values after 50 and 1000 h of aging at 900 °C are presented in Table 2.

4.3. Evolution of γ' morphology during aging at 800, 900 and 950 °C

The morphology of γ' precipitates in various Ni and Co-based superalloys evolves from spheroidal to cuboidal to clover leaves shape [25,40,56,57]. The morphological evolution of γ' precipitates is determined by the balance between the two competing factors of elastic strain energy, arising due to lattice mismatch at the γ/γ' interface, and interfacial energy. For smaller precipitates, the precipitate surface to volume ratio is large and hence the morphology is governed by the dominant interfacial energy. This results in the evolution of spheroidal shape of the γ' precipitates. On the other hand, when precipitates coarsen, the surface to volume ratio becomes small and the dominant elastic strain energy governs the morphology of the precipitates. Generally, in Ni and Co-based superalloys, where precipitates are stiffer than the matrix, the γ' precipitates grow along the elastically soft direction of [100], in order to minimize the elastic strain energy, and hence evolves in to a cuboidal shape [6,21,40,58].

In the present study, the mode value of PDF for the 2W alloy remains close to 1.5, which is close to the defined value of $\sqrt{2}$ for the cuboidal shape precipitates, during aging duration between 50 and 1000 h at the aging temperatures of 800, 900 and 950 °C. This indicates that the γ' precipitate shape in the 2 W alloy remains cuboidal and the γ' precipitate distributed randomly in the γ matrix till aging duration of 1000 h between 800 and 950 °C. We believe that an addition of W to the 0W alloy is playing an important role in stabilizing the cuboidal morphology of γ' precipitates.

Table 4

Comparison of coarsening rate constant values of the present alloy (2W) with other reported Co and Ni-based superalloys.

Alloy	Temperature (°C)	Rate constant (K_r , m^3/s)	References
CMSX-4	900	6.86×10^{-27}	[61]
	950	22.1×10^{-27}	
Co-10Al-10W	900	1.41×10^{-27}	[34]
Co-10Al-5W-2Ta	900	1.04×10^{-27}	[43]
Co-8.8Al-7.3W	900	0.55×10^{-27}	[44]
Co-9.1Al-7W	900	0.67×10^{-27}	[62]
Co-9Al-9W-10Ni	900	0.89×10^{-27}	[64]
Co-5.6Al-5.8W-6.6Ti-0.12B	900	15×10^{-27}	[63]
	950	40×10^{-27}	
Co-9.7Al-7.1W-2.1Ru	900	0.27×10^{-27}	[44]
Co-30Ni-10Al-5Mo-2Nb-2Re	900	1.13×10^{-27}	[27]
Co-10Ni-7Al-4Ti-2W-3Mo-1Nb-1Ta	900	3.9×10^{-27}	[20]
Co-30Ni-7Al-4Ti-2W-3Mo-1Nb-1Ta	900	3.8×10^{-27}	
Co-30Ni-10Al-3Mo-2Ta-2Ti-2W (2W)	900	5.8×10^{-27}	Present study

Table 5Activation energy for γ' precipitate coarsening in various Co and Ni-based superalloys.

Alloy	Temperature range (°C)	Activation energy (kJ/mol)	References
Co-10Al-10W (at%)	800-900	295	[34]
Co-9Al-9W-10Ni (at%)	650-900	283	[64]
Ni-6.8Al-12Mo-7.6Ta/7.7W (at%)	800-1100	255/251	[69]
Ni-8.8Mo-13.8Al-2.1Ta (at%)	927-1093	268	[70]
Udimet 700	982-1093	270	[71]
Nimonic 80A	750-930	274	[72]
Nimonic 90	750-930	257	[72]
Nimonic 105	750-930	264	[72]
Nimonic PE16	700-850	280	[73]
Inconel 738	750-850	269	[74]
Inconel 939	750-930	266	[72]
CMSX-2	800-1050	260	[75]
CMSX-4	850-1000	272	[61]
Ni-15.5Cr-10.8Co-5.6W-2.1Mo-3.2Al-4.6Ti-0.2Nb-0.4HF-0.08B-0.07C (wt%)	800-900	255	[76]
Co-30Ni-10Al-3Mo-2Ta-2Ti-2W (at%)	800-950	258 ± 6	Present study

4.4. Coarsening exponent, rate constant and activation energy

The temporal exponent of γ' precipitate coarsening was calculated from the slope of the plot between $\log[\langle r(t) \rangle]$ versus $\log(t)$, as shown in Fig. 10(b). The temporal exponent values are calculated to be 0.28 ± 0.03 , 0.23 ± 0.01 and 0.22 ± 0.02 at 800, 900 and 950 °C, respectively. As can be seen, the values, though close to 0.33 as predicted by LSW model for binary, KV model for ternary and PV model for non-dilute multicomponent systems [45,46,59,60], exhibit deviation from the classical matrix diffusion limited coarsening mechanism. However, this most likely indicates that the systems have not achieved a true stationary state and are in the quasi-stationary state. Similar observations were also reported in the Ni-Al-Cr and Ni-Al-Cr-W systems where the exponent values deviate from the model stationary-state prediction [53]. The associated coarsening rate constant values (K_r) were calculated from the slope of the plot between $\langle r(t) \rangle^3$ vs t , as shown in Fig. 10(c). The K_r values for the γ' precipitates in the 2W alloy are calculated to be 0.51 (nm^3/s), 5.80 (nm^3/s) and 15.22 (nm^3/s) at the aging temperatures of 800, 900 and 950 °C, respectively. This indicates an order of magnitude increase in coarsening rate when temperature is increased from 800 to 900 °C. The coarsening rate constant values for a selected set of Co and Ni-based superalloys available in the literature are presented in Table 4 [20,27,34,43,44,61-64]. The rate constant for the present alloy (2W) at 900 °C is comparable to the reported value of 1.41 (nm^3/s) for high W containing Co-10Al-10W alloy [34] and 3.9 (nm^3/s) and 3.8 (nm^3/s) for low W containing Co-10Ni-7Al-4Ti-2W-3Mo-1Nb-1Ta and Co-30Ni-7Al-4Ti-2W-3Mo-1Nb-1Ta alloys, respectively [20]. Thus, the present alloy with low mass density shows comparable γ' precipitate coarsening rate to that observed in other Co-based superalloys with high mass density.

For the matrix diffusion controlled coarsening process, the slowest diffusing solute element in the 2W alloy will govern the coarsening rate.

Assuming that diffusion of element i through the γ -Co matrix will control the coarsening kinetics. The coarsening rate constant is given by the following equation [65]

$$K_r = \frac{8D_i \sigma C_i(1 - C_i)v_m}{9RT(C_i - C_e)^2} \quad (5)$$

where D_i is the diffusion coefficient of element i in the matrix, σ is the precipitate/matrix interfacial energy, v_m is the molar volume of the precipitate, C_e and C_i are the equilibrium solubility of the element i in the matrix and precipitate, respectively, R is universal gas constant and T is the absolute temperature. This equation, in principle allows us to determine the interfacial energy provided that the exponent is 0.33. Recently, this has been attempted for 2W3Mo7Al1Nb1Ta alloy containing 10 and 30 at%Ni (named as L18 and L19) to evaluate the effect of alloying addition on interfacial energy. Unfortunately, both the values (35 and 29.2 mJm^{-2}) have large error bars making any definitive conclusion difficult. Therefore, we have not attempted to estimate the interfacial energy in the present study. However, the retention of aspect ratio of 1.5 for the most of the γ' particle on long duration isothermal heat treatment till 1000 h suggests that interfacial energy is not approaching very low value.

The diffusion coefficient of element i in the γ matrix can be expressed by the following Arrhenius equation

$$D_i = D_{i,0} \exp\left(-\frac{Q_i}{R.T}\right) \quad (6)$$

where $D_{i,0}$ is the pre-exponential factor for element i and Q_i is the activation energy for diffusion of element i in the γ matrix. By using Eqs. (5) and (6), we can arrive at the following equation for the determination of activation energy.

$$\ln\left[\frac{K_r T (C_i - C_e)^2}{D_{i,0} \sigma C_i (1 - C_i) v_m}\right] = \text{Constant} - \frac{Q_i}{RT} \quad (7)$$

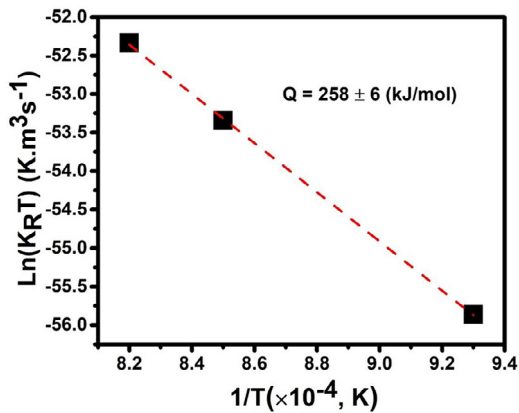


Fig. 11. Arrhenius plot of the coarsening rate constant [$\ln(KT)$] as a function of the inverse of annealing temperature.

Since C_i , C_p , v_m and σ do not vary much with temperature, the activation energy value can be calculated from the slope of the plot between $\ln(KT)$ and $1/T$, as shown in Fig. 11. The calculated activation energy for γ' precipitate coarsening is 258 ± 6 kJ/mol. This value of activation energy is comparable to the activation energy for Mo diffusion in γ -Co (262.0 ± 10.4 kJ/mol) [66,67] and hence, may control the coarsening process. We note that the atoms of Mo with atomic radius of 0.145 nm are larger than other solutes ($r_{Ni} \sim 0.135$ nm, $r_{Al} \sim 0.125$, $r_{Ti} \sim 0.140$ nm, $r_W \sim 0.135$ nm) [68]. Hence, from the diffusion point of view, they are expected to be slow diffusing species. Due to slow diffusion of Mo, a buildup of Mo atoms at the γ/γ' interface has been observed in the 900 °C for 50 h aged condition sample, as was discussed in section 4.2. Our results lead to the conclusion that the γ' precipitate coarsening in the present 2W alloy is controlled by the diffusion of Mo in the γ matrix. A comparison of the activation energies of selected Co and Ni-based superalloys are given in Table 5 [34,61,64,69–76]. The activation energies of γ' precipitate coarsening of superalloys are in the range of 250 – 300 kJ/mole and the activation energy for the present alloy (2W) lies in this range.

5. Conclusions

In summary, the present work elucidates the effect of W addition on microstructural evolution, γ' solvus temperature and long-term stability in a series of Co-30Ni-10Al-(5-x) Mo-2Ta-2Ti-xW at% alloys. The following major points can be drawn from the present work.

1. All the W containing alloys show duplex γ/γ' microstructure with cuboidal γ' precipitates uniformly embedded in the γ matrix. An addition of 0.5 at% W in place of Mo to the 0W alloy increases the γ' volume fraction from 62 ± 2 (%) to 72 ± 4 (%).
2. Replacement of 2 at% of Mo with an equal amount of W in the 0W alloy increases the γ' solvus temperature by 60 °C from 1070 °C to 1130 °C and γ' volume fraction from 65 ± 2 to 75 ± 2 (%).
3. The APT analysis of the 2W alloy aged at 900 °C for 50 h shows a strong partitioning of Ta and Ti in the γ' phase with partitioning coefficients of $K_{Ta} = 4.93$ and $K_{Ti} = 3.05$ while W, Ni and Al show a relatively weak partitioning with partitioning coefficients of $K_W = 2.01$, $K_{Ni} = 1.36$ and $K_{Al} = 1.70$. Additionally, the partitioning preference of Mo changes from the γ' phase in 0W alloy to equally in both γ and γ' phases in 2W alloy. An interfacial segregation of Mo atoms has been observed at the γ/γ' interface that may result in a decrease of interfacial free energy. The segregation almost disappears on long time (1000 h) exposure at high temperature (900 °C).
4. 2W alloy shows good microstructural stability with γ' morphology remains cuboidal till 1000 h of heat-treatment at the aging temperatures of 800 , 900 and 950 °C.

5. The temporal exponents of γ' precipitate size evolution during coarsening of the 2W alloy deviate slightly from the predicted theoretical value of 0.33 , as predicted by modified LSW based model, thus suggesting the systems are in a quasi-stationary state.
6. The coarsening rate constant values (K_r) for γ' precipitate, as obtained by modified LSW based coarsening model, are estimated to be 0.51 , 5.80 and 15.22 at the aging temperatures of 800 , 900 and 950 °C. The K_r value at 900 °C is comparable to the high density W containing Co-Al-W alloys. Activation energy for γ' precipitate coarsening is estimated to be 258 ± 6 kJ/mol, which compares well with that for the diffusion of Mo in γ -Co. This result suggests that γ' precipitate coarsening is controlled by diffusion of Mo in the γ matrix.

Declaration of Competing Interest

None.

Acknowledgments

The authors would like to acknowledge the microscopy facility available at the Advanced Facility for Microscopy and Microanalysis (AFMM) center, Indian Institute of Science, Bangalore. KC is grateful for the financial support from Department of Science and Technology (DST) in the form of J.C. Bose national fellowship. KC also acknowledges the Gas Turbine Materials and Processes (GTMAP) program of Aeronautics Research and Development Board, DRDO for the financial support. The authors are grateful to U. Tezins and A. Sturm for their technical support of the atom probe tomography and focused ion beam facilities at the Max-Planck-Institut für Eisenforschung. SKM acknowledges financial support from the Alexander von Humboldt Foundation.

Supplementary materials

Supplementary material associated with this article can be found, in the online version, at doi:[10.1016/j.mtla.2020.100632](https://doi.org/10.1016/j.mtla.2020.100632).

References

- [1] R.C. Reed, The Superalloys: Fundamentals and Applications, Cambridge University Press, 2008, doi:[10.1017/CBO9780511541285](https://doi.org/10.1017/CBO9780511541285).
- [2] T.M. Pollock, A.S. Argon, Creep resistance of CMSX-3 nickel base superalloy single crystals, *Acta Metall. Mater.* 40 (1992) 1–30, doi:[10.1016/0956-7151\(92\)90195-K](https://doi.org/10.1016/0956-7151(92)90195-K).
- [3] J.H. Perepezko, The hotter the engine, the better, *Science* 326 (2009) 1068–1069, doi:[10.1126/science.1179327](https://doi.org/10.1126/science.1179327).
- [4] T.M. Pollock, Alloy design for aircraft engines, *Nat. Mater.* 15 (2016) 809–815, doi:[10.1038/nmat4709](https://doi.org/10.1038/nmat4709).
- [5] C.S. Lee, Precipitation-hardening Characteristics of Ternary Cobalt-aluminum-X Alloys, (1971). http://arizona.openrepository.com/arizona/bitstream/10150/287709/1/azu_td_7124368_sipl_1_m.pdf (accessed June 23, 2017).
- [6] J. Sato, T. Omori, K. Oikawa, I. Ohnuma, R. Kainuma, K. Ishida, Cobalt-base high-temperature alloys, *Science* 312 (2006) 90–91, doi:[10.1126/science.1121738](https://doi.org/10.1126/science.1121738).
- [7] T.M. Pollock, J. Dibbern, M. Tsunekane, J. Zhu, A. Suzuki, New co-based γ/γ' high-temperature alloys, *JOM* 62 (2010) 58–63, doi:[10.1007/s11837-010-0013-y](https://doi.org/10.1007/s11837-010-0013-y).
- [8] J. Koßmann, C.H. Zenk, I. Lopez-Galilea, S. Neumeier, A. Kostka, S. Huth, W. Theisen, M. Göken, R. Drautz, T. Hammerschmidt, Microsegregation and precipitates of an as-cast co-based superalloy—microstructural characterization and phase stability modelling, *J. Mater. Sci.* 50 (2015) 6329–6338, doi:[10.1007/s10853-015-9177-8](https://doi.org/10.1007/s10853-015-9177-8).
- [9] D.L. Douglass, V.S. Bhide, E. Vineberg, The corrosion of some superalloys in contact with coal chars in coal gasifier atmospheres, *Oxid. Met.* 16 (1981) 29–79, doi:[10.1007/BF00603744](https://doi.org/10.1007/BF00603744).
- [10] A.K. Misra, Corrosion of metals and alloys in sulfate melts at 750 °C, *Oxid. Met.* 25 (1986) 373–396, doi:[10.1007/BF01072916](https://doi.org/10.1007/BF01072916).
- [11] S. Kobayashi, Y. Tsukamoto, T. Takasugi, H. Chinen, T. Omori, K. Ishida, S. Zaefferer, Determination of phase equilibria in the co-rich co-al-w ternary system with a diffusion-couple technique, *Intermetallics* 17 (2009) 1085–1089, doi:[10.1016/j.intermet.2009.05.009](https://doi.org/10.1016/j.intermet.2009.05.009).
- [12] F. Xue, H.J. Zhou, Q.Y. Shi, X.H. Chen, H. Chang, M.L. Wang, Q. Feng, Creep behavior in a γ' strengthened co-al-w-ta-ti single-crystal alloy at 1000 °C, *Scr. Mater.* 97 (2015) 37–40, doi:[10.1016/j.scriptamat.2014.10.015](https://doi.org/10.1016/j.scriptamat.2014.10.015).
- [13] M. Ooshima, K. Tanaka, N.L. Okamoto, K. Kishida, H. Inui, Effects of quaternary alloying elements on the γ' solvus temperature of co-al-w based alloys with fcc/L1₂ two-phase microstructures, *J. Alloys Compd.* 508 (2010) 71–78, doi:[10.1016/j.jallcom.2010.08.050](https://doi.org/10.1016/j.jallcom.2010.08.050).

- [14] L. Shi, J.J. Yu, C.Y. Cui, X.F. Sun, Effect of ta additions on microstructure and mechanical properties of a single-crystal co-al-w-base alloy, *Mater. Lett.* 149 (2015) 58–61, doi:10.1016/j.matlet.2015.01.133.
- [15] A. Bauer, S. Neumeier, F. Pyczak, R.F. Singer, M. Göken, Creep properties of different γ' -strengthened co-based superalloys, *Mater. Sci. Eng.: A* 550 (2012) 333–341, doi:10.1016/j.msea.2012.04.083.
- [16] C.H. Zenk, S. Neumeier, H.J. Stone, M. Göken, Mechanical properties and lattice misfit of γ/γ' strengthened co-base superalloys in the co-w-al-ti quaternary system, *Intermetallics* 55 (2014) 28–39, doi:10.1016/j.intermet.2014.07.006.
- [17] P.J. Boccini, C.K. Sudbrack, D.J. Sauza, R.D. Noebe, D.N. Seidman, D.C. Dunand, Effect of tungsten concentration on microstructures of co-10ni-6al-(0,2,4,6)w-6ti (at%) cobalt-based superalloys, *Mater. Sci. Eng.: A* 700 (2017) 481–486, doi:10.1016/j.msea.2017.06.018.
- [18] I. Povstugar, P.-P. Choi, S. Neumeier, A. Bauer, C.H. Zenk, M. Göken, D. Raabe, Elemental partitioning and mechanical properties of Ti- and Ta-containing co-al-w-base superalloys studied by atom probe tomography and nanoindentation, *Acta Mater.* 78 (2014) 78–85, doi:10.1016/j.actamat.2014.06.020.
- [19] P.J. Boccini, C.K. Sudbrack, R.D. Noebe, D.C. Dunand, D.N. Seidman, Effects of titanium substitutions for aluminum and tungsten in Co-10Ni-9Al-9W (at%) superalloys, *Mater. Sci. Eng.: A* 705 (2017) 122–132, doi:10.1016/j.msea.2017.08.034.
- [20] E.A. Lass, D.J. Sauza, D.C. Dunand, D.N. Seidman, Multicomponent γ' -strengthened co-based superalloys with increased solvus temperatures and reduced mass densities, *Acta Mater.* 147 (2018) 284–295, doi:10.1016/j.actamat.2018.01.034.
- [21] S.K. Makineni, A. Samanta, T. Rojhirunsakool, T. Alam, B. Nithin, A.K. Singh, R. Banerjee, K. Chattopadhyay, A new class of high strength high temperature cobalt based γ/γ' co-mo-al alloys stabilized with ta addition, *Acta Mater.* 97 (2015) 29–40, doi:10.1016/j.actamat.2015.06.034.
- [22] S.K. Makineni, B. Nithin, K. Chattopadhyay, A new tungsten-free γ/γ' co-al-mo-nb-based superalloy, *Scr. Mater.* 98 (2015) 36–39, doi:10.1016/j.scriptamat.2014.11.009.
- [23] S.K. Makineni, B. Nithin, K. Chattopadhyay, Synthesis of a new tungsten-free γ/γ' cobalt-based superalloy by tuning alloying additions, *Acta Mater.* 85 (2015) 85–94, doi:10.1016/j.actamat.2014.11.016.
- [24] S.K. Makineni, B. Nithin, D. Palanisamy, K. Chattopadhyay, Phase evolution and crystallography of precipitates during decomposition of new “tungsten-free” co(ni)-mo-al-nb γ/γ' superalloys at elevated temperatures, *J. Mater. Sci.* 51 (2016) 7843–7860, doi:10.1007/s10853-016-0026-1.
- [25] P. Pandey, S.K. Makineni, A. Samanta, A. Sharma, S.M. Das, B. Nithin, C. Srivastava, A.K. Singh, D. Raabe, B. Gault, K. Chattopadhyay, Elemental site occupancy in the L12 A3B ordered intermetallic phase in co-based superalloys and its influence on the microstructure, *Acta Mater.* 163 (2019) 140–153, doi:10.1016/j.actamat.2018.09.049.
- [26] B. Nithin, K. Chattopadhyay, G. Phanikumar, Characterization of the hot deformation behavior and microstructure evolution of a new γ/γ' strengthened cobalt-based superalloy, *Metall. Mater. Trans. A* 49 (2018) 4895–4905, doi:10.1007/s11661-018-4795-9.
- [27] P. Pandey, A.K. Sawant, B. Nithin, Z. Peng, S.K. Makineni, B. Gault, K. Chattopadhyay, On the effect of re addition on microstructural evolution of a coni-based superalloy, *Acta Mater.* (2019), doi:10.1016/j.actamat.2019.01.046.
- [28] F. Pyczak, A. Bauer, M. Göken, U. Lorenz, S. Neumeier, M. Oehring, J. Paul, N. Schell, A. Schreyer, A. Stark, F. Symanzik, The effect of tungsten content on the properties of L12-hardened co-al-w alloys, *J. Alloys Compd.* 632 (2015) 110–115, doi:10.1016/j.jallcom.2015.01.031.
- [29] K. Thompson, D. Lawrence, D.J. Larson, J.D. Olson, T.F. Kelly, B. Gorman, In situ site-specific specimen preparation for atom probe tomography, *Ultramicroscopy* 107 (2007) 131–139, doi:10.1016/j.ultramic.2006.06.008.
- [30] S.K. Makineni, M. Lenz, P. Kontis, Z. Li, A. Kumar, P.J. Felfer, S. Neumeier, M. Herbig, E. Speicker, D. Raabe, B. Gault, Correlative microscopy—novel methods and their applications to explore 3D chemistry and structure of nanoscale lattice defects: a case study in superalloys, *JOM* (2018), doi:10.1007/s11837-018-2802-7.
- [31] ASTM B311-17, Standard Test Method for Density of Powder Metallurgy (Pm) Materials Containing Less Than Two Percent Porosity, (2017).
- [32] Y. Amouyal, Z. Mao, C. Booth-Morrison, D.N. Seidman, On the interplay between tungsten and tantalum atoms in ni-based superalloys: an atom-probe tomographic and first-principles study, *Appl. Phys. Lett.* 94 (2009) 041917, doi:10.1063/1.3073885.
- [33] S. Meher, H.-Y. Yan, S. Nag, D. Dye, R. Banerjee, Solute partitioning and site preference in γ/γ' cobalt-base alloys, *Scr. Mater.* 67 (2012) 850–853, doi:10.1016/j.scriptamat.2012.08.006.
- [34] S. Meher, S. Nag, J. Tiley, A. Goel, R. Banerjee, Coarsening kinetics of γ' precipitates in cobalt-base alloys, *Acta Mater.* 61 (2013) 4266–4276, doi:10.1016/j.actamat.2013.03.052.
- [35] S. Meher, R. Banerjee, Partitioning and site occupancy of ta and mo in co-base γ/γ' alloys studied by atom probe tomography, *Intermetallics* 49 (2014) 138–142, doi:10.1016/j.intermet.2014.01.020.
- [36] E.A. Lass, D.J. Sauza, D.C. Dunand, D.N. Seidman, Multicomponent γ' -strengthened co-based superalloys with increased solvus temperatures and reduced mass densities, *Acta Mater.* 147 (2018) 284–295, doi:10.1016/j.actamat.2018.01.034.
- [37] C. Jiang, First-principles study of Co₃(Al,W) alloys using special quasi-random structures, *Scr. Mater.* 59 (2008) 1075–1078, doi:10.1016/j.scriptamat.2008.07.021.
- [38] J.E. Saal, C. Wolverton, Thermodynamic stability of co-al-w L12 γ' , *Acta Mater.* 61 (2013) 2330–2338, doi:10.1016/j.actamat.2013.01.004.
- [39] H. Baker, *Alloy Phase Diagram*, ASM, 1992.
- [40] C. Booth-Morrison, R.D. Noebe, D.N. Seidman, Effects of tantalum on the temporal evolution of a model ni-al-cr superalloy during phase decomposition, *Acta Mater.* 57 (2009) 909–920, doi:10.1016/j.actamat.2008.10.029.
- [41] K.E. Yoon, R.D. Noebe, D.N. Seidman, Effects of rhenium addition on the temporal evolution of the nanostructure and chemistry of a model ni-cr-al superalloy. I: experimental observations, *Acta Mater.* 55 (2007) 1145–1157, doi:10.1016/j.actamat.2006.08.027.
- [42] K.E. Yoon, R.D. Noebe, D.N. Seidman, Effects of rhenium addition on the temporal evolution of the nanostructure and chemistry of a model ni-cr-al superalloy. II: analysis of the coarsening behavior, *Acta Mater.* 55 (2007) 1159–1169, doi:10.1016/j.actamat.2006.08.024.
- [43] V.A. Vorontsov, J.S. Barnard, K.M. Rahman, H.-Y. Yan, P.A. Midgley, D. Dye, Coarsening behaviour and interfacial structure of γ' precipitates in co-al-w based superalloys, *Acta Mater.* 120 (2016) 14–23, doi:10.1016/j.actamat.2016.08.023.
- [44] D.J. Sauza, P.J. Boccini, D.C. Dunand, D.N. Seidman, Influence of ruthenium on microstructural evolution in a model co al w superalloy, *Acta Mater.* 117 (2016) 135–145, doi:10.1016/j.actamat.2016.07.014.
- [45] I.M. Lifshitz, V.V. Slyozov, The kinetics of precipitation from supersaturated solid solutions, *J. Phys. Chem. Solids* 19 (1961) 35–50, doi:10.1016/0022-3697(61)90054-3.
- [46] C.Z. Wagner, Z. Elektrochem, Theory of precipitate change by redissolution, *Angew. Phys. Chem.* 65 (1961) 581–591.
- [47] A.J. Ardell, V. Ozolins, Trans-interface diffusion-controlled coarsening, *Nat. Mater.* 4 (2005) 309–316, doi:10.1038/nmat1340.
- [48] A.J. Ardell, Trans-interface-diffusion-controlled coarsening of γ' precipitates in ternary ni-al-cr alloys, *Acta Mater.* 61 (2013) 7828–7840, doi:10.1016/j.actamat.2013.09.021.
- [49] J.R. Davis, K. Mills, S. Lampman, *ASM Handbook*. Vol. 1. *Properties and Selection: Irons, Steels, and High-Performance Alloys*, Met. Park OH ASM Int. (1990).
- [50] S.K. Makineni, A. Samanta, T. Rojhirunsakool, T. Alam, B. Nithin, A.K. Singh, R. Banerjee, K. Chattopadhyay, A new class of high strength high temperature cobalt based γ/γ' co-mo-al alloys stabilized with ta addition, *Acta Mater.* 97 (2015) 29–40, doi:10.1016/j.actamat.2015.06.034.
- [51] P.J. Boccini, C.K. Sudbrack, D.J. Sauza, R.D. Noebe, D.N. Seidman, D.C. Dunand, Effect of tungsten concentration on microstructures of co-10ni-6al-(0,2,4,6)w-6ti (at%) cobalt-based superalloys, *Mater. Sci. Eng.: A* 700 (2017) 481–486, doi:10.1016/j.msea.2017.06.018.
- [52] P.A.J. Bagot, O.B.W. Silk, J.O. Douglas, S. Pedrazzini, D.J. Crudden, T.L. Martin, M.C. Hardy, M.P. Moody, R.C. Reed, An atom probe tomography study of site preference and partitioning in a nickel-based superalloy, *Acta Mater.* 125 (2017) 156–165, doi:10.1016/j.actamat.2016.11.053.
- [53] C.K. Sudbrack, T.D. Ziebell, R.D. Noebe, D.N. Seidman, Effects of a tungsten addition on the morphological evolution, spatial correlations and temporal evolution of a model ni-al-cr superalloy, *Acta Mater.* 56 (2008) 448–463, doi:10.1016/j.actamat.2007.09.042.
- [54] Y. Amouyal, Z. Mao, D.N. Seidman, Effects of tantalum on the partitioning of tungsten between the γ - and γ' -phases in nickel-based superalloys: linking experimental and computational approaches, *Acta Mater.* 58 (2010) 5898–5911, doi:10.1016/j.actamat.2010.07.004.
- [55] P.J. Boccini, E.A. Lass, K.-W. Moon, M.E. Williams, C.E. Campbell, U.R. Kattnar, D.C. Dunand, D.N. Seidman, Atom-probe tomographic study of γ/γ' interfaces and compositions in an aged co-al-w superalloy, *Scr. Mater.* 68 (2013) 563–566, doi:10.1016/j.scriptamat.2012.11.035.
- [56] Y. Chen, R. Prasath babu, T.J.A. Slater, M. Bai, R. Mitchell, O. Ciucu, M. Preuss, S.J. Haigh, An investigation of diffusion-mediated cyclic coarsening and reversal coarsening in an advanced ni-based superalloy, *Acta Mater.* 110 (2016) 295–305, doi:10.1016/j.actamat.2016.02.067.
- [57] J.S. Van Sluytman, T.M. Pollock, Optimal precipitate shapes in nickel-base γ/γ' alloys, *Acta Mater.* 60 (2012) 1771–1783, doi:10.1016/j.actamat.2011.12.008.
- [58] S.K. Makineni, M. Lenz, S. Neumeier, E. Spiecker, D. Raabe, B. Gault, Elemental segregation to antiphase boundaries in a crept coni-based single crystal superalloy, *Scr. Mater.* 157 (2018) 62–66, doi:10.1016/j.scriptamat.2018.07.042.
- [59] C.J. Kuehmann, P.W. Voorhees, Ostwald ripening in ternary alloys, *MMTA* 27 (1996) 937–943, doi:10.1007/BF02649761.
- [60] T. Philippe, P.W. Voorhees, Ostwald ripening in multicomponent alloys, *Acta Mater.* 61 (2013) 4237–4244, doi:10.1016/j.actamat.2013.03.049.
- [61] J. Lapin, M. Gebura, T. Pelachová, M. Nazmy, Coarsening kinetics of cuboidal γ precipitates in single crystal nickel base superalloy CMSX-4, *Kovore Mater.* 46 (2008) 313–322.
- [62] A. Azzam, T. Philippe, A. Hauet, F. Danoix, D. Locq, P. Caron, D. Blavette, Kinetics pathway of precipitation in model co-al-w superalloy, *Acta Mater.* 145 (2018) 377–387, doi:10.1016/j.actamat.2017.12.032.
- [63] D.J. Sauza, D.C. Dunand, D.N. Seidman, Microstructural evolution and high-temperature strength of a γ (f.c.c.)/ γ' (L12) co-al-w-ti-b superalloy, *Acta Mater.* 174 (2019) 427–438, doi:10.1016/j.actamat.2019.05.058.
- [64] D.J. Sauza, D.C. Dunand, R.D. Noebe, D.N. Seidman, γ' (L12) precipitate evolution during isothermal aging of a coalwni superalloy, *Acta Mater.* 164 (2019) 654–662, doi:10.1016/j.actamat.2018.11.01.
- [65] H.A. Calderon, P.W. Voorhees, J.L. Murray, G. Kostorz, Ostwald ripening in concentrated alloys, *Acta Metall. Mater.* 42 (1994) 991–1000, doi:10.1016/0956-7151(94)90293-3.
- [66] S. Neumeier, H.U. Rehman, J. Neuner, C.H. Zenk, S. Michel, S. Schuwallow, J. Rogal, R. Drautz, M. Göken, Diffusion of solutes in fcc cobalt investigated by diffusion couples and first principles kinetic monte carlo, *Acta Mater.* 106 (2016) 304–312, doi:10.1016/j.actamat.2016.01.028.
- [67] L. Habraken, V. Leroy, D. Coutsouradis, A. Davin, Diffusion de quelques éléments de substitution dans le fer, le nickel et le cobalt, *Mem. Sci. Rev. Met.* 60 (1963) 275–283.

- [68] J.C. Slater, Atomic radii in crystals, *J. Chem. Phys.* 41 (1964) 3199–3204, doi:[10.1063/1.1725697](https://doi.org/10.1063/1.1725697).
- [69] S. Sadiq, D.R.F. West, The coarsening of γ' particles in ni al mo ta and ni al mo w alloys, *Scr. Metall.* 19 (1985) 833–837, doi:[10.1016/0036-9748\(85\)90202-9](https://doi.org/10.1016/0036-9748(85)90202-9).
- [70] R.A. MacKay, M.V. Nathal, γ' coarsening in high volume fraction nickel-base alloys, *Acta Metall. Mater.* 38 (1990) 993–1005, doi:[10.1016/0956-7151\(90\)90171-C](https://doi.org/10.1016/0956-7151(90)90171-C).
- [71] E.H. Van der Molen, J.M. Oblak, O.H. Krieger, Control of γ' particle size and volume fraction in the high temperature superalloy udimet 700, *Metall. Trans. 2* (1971) 1627–1633, doi:[10.1007/BF02913886](https://doi.org/10.1007/BF02913886).
- [72] P.K. Footner, B.P. Richards, Long — term growth of superalloy γ' particles, *J. Mater. Sci.* 17 (1982) 2141–2153, doi:[10.1007/BF00540433](https://doi.org/10.1007/BF00540433).
- [73] K. Bhanu Sankara Rao, V. Seetharaman, S.L. Mannan, P. Rodriguez, Effect of long-term exposure at elevated temperatures on the structure and properties of a nimonic pe 16 superalloy, *Mater. Sci. Eng.* 58 (1983) 93–106, doi:[10.1016/0025-5416\(83\)90140-4](https://doi.org/10.1016/0025-5416(83)90140-4).
- [74] R.A. Stevens, P.E.J. Flewitt, The effects of γ' precipitate coarsening during isothermal aging and creep of the nickel-base superalloy IN-738, *Mater. Sci. Eng.* 37 (1979) 237–247, doi:[10.1016/0025-5416\(79\)90157-5](https://doi.org/10.1016/0025-5416(79)90157-5).
- [75] A.M. Ges, O. Fornaro, H.A. Palacio, Coarsening behaviour of a ni-base superalloy under different heat treatment conditions, *Mater. Sci. Eng.: A* 458 (2007) 96–100, doi:[10.1016/j.msea.2006.12.107](https://doi.org/10.1016/j.msea.2006.12.107).
- [76] J.S. Hou, J.T. Guo, Influence of thermal exposure on the microstructures and mechanical properties of a superalloy, *J. Mater. Eng. Perform.* 15 (2006) 67–75, doi:[10.1361/105994906X83501](https://doi.org/10.1361/105994906X83501).